Available online at www.sciencedirect.com
SCIENCE DIRECT®
Journal of Chromatography A, 1033 (2004) 257–266
JOURNAL OF CHROMATOGRAPHY A
www.elsevier.com/locate/chroma

Comparison between different sheathless electrospray emitter configurations regarding the performance of nanoscale liquid chromatography–time-of-flight mass spectrometry analysis

Ardeshir Amirkhani, Magnus Wetterhall, Stefan Nilsson, Rolf Danielsson, Jonas Bergquist*

Department of Analytical Chemistry, Institute of Chemistry, Uppsala University, P.O. Box 599, SE-75124 Uppsala, Sweden

Received 26 November 2003; accepted 29 January 2004

Abstract

Four different sheathless electrospray ionization (ESI) configurations were investigated for a nano liquid chromatography (LC) system. The studied configurations were: a column with an integrated emitter, with the ESI potential applied before or after the column, and a column with separate emitter, with the ESI voltage applied at a union before the emitter or at the emitter tip. The results indicates that the efficiency of the LC system is rather independent of the configuration when using 95 μm i.d. columns, acetic mobile phase and standard peptides as a sample. Introduction of post column dead volume seems not to be a critical issue at least with flow rates down to 600 nl/min.

Keywords: Electrospray ionization; Band broadening; Principal component analysis; Instrumentation; Peptides

1. Introduction

Miniaturized liquid chromatography (LC) has established itself as a complementary separation technique to conventional LC. This is mainly owing to lower sample volume requirements, lower flow rates and enhanced detection performance with the use of concentration sensitive detectors [1]. Furthermore, the lower flow rate is well suited for electrospray ionization (ESI) followed by mass spectrometric detection. The ESI mass spectrometry (MS) signal, however, can be affected by changes in the sample flow rate and is therefore not considered as a pure concentration sensitive detector [2–4]. The effect of the flow rate is highly dependent on the interface characteristics [2]. It has been shown that a pure ESI-MS can behave as a mass flow sensitive detector at flow rates below 400 nl/min [4].

In addition, the extra-column band broadening effects on the separation is also influenced by the lower flow rates [1,5]. This band broadening, introduced by dead volumes and flow distortion, can be divided into pre-column and post-column contributions. The pre-column contributions can be minimized by the use of on-line pre-concentration, as for instance using diluted samples dissolved in a weak solvent (water in reversed-phase LC) in combination with a gradient elution [6]. Column switching techniques can also be employed for on-line pre-concentration and desalting of a sample [7–9]. Thus, pre-column band broadening can be eliminated. It is then necessary to minimize the post-column band broadening caused by the column outlet frit, connecting tubing and the electrospray emitter. These parameters are, more or less, determined by the ESI interface used.

Various electrospray systems for nanoscale LC and capillary electrophoresis (CE) working in the nl–μl/min range have been designed [2,10]. Fused silica capillary emitters have often been used for such interfaces, since they are quite durable, non reactive, inexpensive and mostly important available in various internal and outer diameters. The fused silica emitter may be pulled, grinded or etched to a sharp tip in order to optimize the spray performance [11–13]. Another consideration is the management of connection points for the ESI potential, since the fused silica is nonconductive. The high voltage at the capillary spray tip is applied to the eluting mobile phase in either of two ways; by coating the fused silica capillaries with a conductive material [14] or by the introduction of a liquid contact with a conductive material at some point before the spray tip [4].

* Corresponding author. Tel.: +46-18-471-3675; fax: +46-18-471-3692.
E-mail address: jonas.bergquist@kemi.uu.se (J. Bergquist).

0021-9673/$ – see front matter © 2004 Elsevier B.V. All rights reserved.
doi:10.1016/j.chroma.2004.01.063

The choice of connection points for the ESI potential and counter electrode can have dramatic effects on the analytes and the separation [15,16].

In this study, the relation between the flow rate and peak stability as well as peak intensity at different concentrations of an analyte was investigated for sheathless electrospray. Several nanoscale columns with separate electrospray emitters and integrated electrospray emitters made from fused-silica capillaries as well as different connection points for the high voltage were investigated regarding the performance of the nanoLC system. In addition, a tryptic digest of bovine serum albumin (BSA) was analyzed in one of the configurations to evaluate its performance for a more complex sample.

2. Experimental

2.1. Materials

Acetonitrile, formic acid, diiodomethane, and trichloroethylene were purchased from Merck (Darmstadt, Germany). All used chemicals were of analytical grade. The peptide standards leucine–enkephalin (M_r 555.6), Bradykinin fragment 1–5 (572.7), methionine–enkephalin (573.7), oxytocin (1007.2), angiotensin II (1046.2), bradykinin (1060.2), Arg^8-vasopressin (1084.2), luteinizing hormone-releasing hormone (LHRH, 1182.3), substance P (1347.6), bombesin (1619.9) as well as urea, ammonium-carbonate, iodoacetamide and the protein BSA (66 397.9) were obtained from Sigma (St. Louis, MO, USA) and were used without further purification. Dithiothreitol was purchased from Amersham Biosciences (Uppsala, Sweden). Trypsin, sequence grade from bovine pancreas (1,418,475), was obtained from Roche Diagnostics (Penzberg, Germany). Polyimide sealing resin used for the ESI emitter production was obtained from Alltech (Deerfield, IL, USA). Graphite powder, 1–2 μm particle size, used for the ESI emitter, was obtained from Aldrich (Milwaukee, WI, USA). Water was purified with a Milli-Q purification system (Millipore, Bedford, MA, USA). All fused-silica capillaries were obtained from Polymicro Technologies (Phoenix, AZ, USA).

2.2. Emitter configurations

Two different kinds of nanoscale columns, one with an on-column integrated ESI emitter [14] and the other with a separate electrospray emitter, were constructed. The nanoLC capillaries with an on-column integrated emitter were used for experiments in which the electrospray voltage was applied at the outlet end (Fig. 1A) as well as at the inlet end of the capillary (Fig. 1B). Experiments were also conducted using nanoscale LC columns with a separate emitter where the electrospray voltage was applied on the tip of the separate emitter (Fig. 1C) or at the union between the LC column and the separate emitter (Fig. 1D) as a liquid junction.

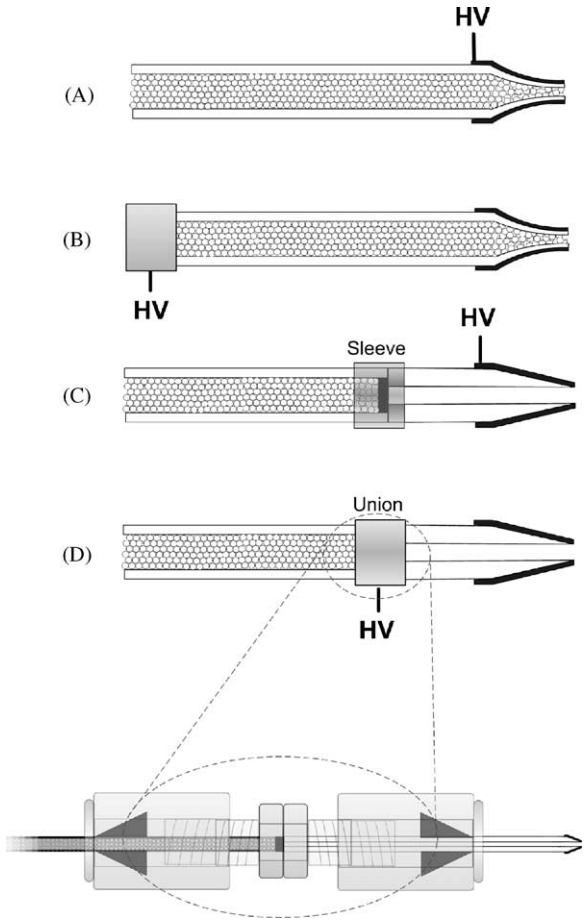

Fig. 1. Schematic drawings of the different nanoLC-column configurations. A and B represent columns with integrated emitters while C and D represent separate columns and emitters. The electrospray voltage was applied at the outlet end in configuration A and at inlet end of the column in configuration B. In C, the electrospray voltage was applied at the outlet end of the emitter while in D, the electrospray voltage was applied via a union between the column and emitter.

2.2.1. On-column integrated ESI emitter (A and B)

Fused-silica capillaries (22 cm × 360 μm o.d. × 95 μm i.d.) were cut and the ESI emitter end was pulled manually to a fine tip using an electric arc generated by an optical fiber splicer instrument (model PFS-200, Little Rock, AR, USA). The pulled tip functioned as the ESI emitter tip as well as the restrictor for the stationary phase particles, thus no additional frits were employed to retain the adsorption media in the column. The pulled emitter tip was visually estimated (compared with 25 μm i.d. fused-silica capillary using the optical fiber splicer instrument) to have an orifice i.d. of 20–25 μm before the coating procedure. The emitter ends of the integrated columns were coated with a conductive mixture of polyimide/graphite according to the "Black Dust" method [17] prior to column preparation. The columns with integrated emitters were later used for the construction of nanoLC–ESI according to configurations A and B (see Fig. 1).

2.2.2. Separate ESI emitter (C and D)

The separate ESI emitter was produced by manually tapering fused silica capillaries (10 cm × 360 μm o.d. × 25 μm i.d.) following a protocol described by Barnidge et al. [12]. Briefly, a fused-silica capillary was cut and loaded into a pin-vise holder through a piece of PTFE tubing. The pin-vise, holding the capillary, was inserted in a hand-held drill and the capillary tip was rotated onto a piece of waterproof silicon carbide paper no. 800 (Struers, Rodovre, Denmark) mounted on a piece of circular plastic that was rotating in a drill press. The tips were subjected to shaping for a minute, and were subsequently ready for the application of the conductive "Black Dust" coating.

The emitters were later used for the construction of nanoLC–ESI according to configuration C and D (see Fig. 1). The emitter and the column in configuration C were connected via a Teflon™ sleeve (5 mm × 0.3 mm i.d.) and in configuration D via a stainless steel stainless steel union, 0.4 mm i.d. (SGE, Victoria, Australia). The blunt end of the emitter and the column outlet end were inserted into the sleeve or the union and connected to each other with zero dead volume as inspected by a microscope.

2.3. Preparation of capillary column

Nanoscale columns, with separate electrospray emitters and on-column integrated electrospray emitters, were slurry packed in the laboratory with 3 μm C_2/C_{18} particles, 120 Å pore size (μRPC, Amersham Biosciences, UK) in fused silica, 22 cm × 360 μm o.d. × 95 μm i.d. A 5% (w/w) slurry of the packing material in diiodomethane–trichloroethylene (38:62, v/v) was homogenized in an ultrasonic bath for approximately 1 min. This slurry solvent was selected, as its density is very similar to that of the silica particles [18]. A packing reservoir connected to an empty capillary was filled with the slurry.

The outlet end of the capillary was provided with a frit by carefully pushing and spinning the capillary on a wet piece of glass fiber paper (Whatman GF/A, W & R Balston, UK). Wetting the glass fiber paper with ethanol made the fritting procedure more successful. The fritted end of the capillary was fitted against a 5 cm long fused silica capillary (360 μm o.d. × 50 μm i.d.) used as a restrictor inside a Teflon sleeve. The fritted end of the capillary and the restrictor capillary were inserted into the sleeve and connected to each with zero dead volume.

The integrated columns were packed without any frits or restrictor capillary. The packing procedure was initiated by delivering 0.1 ml/min acetonitrile into the reservoir until the pressure reached 450 bar using an LC pump (PU-980, Jasco, Tokyo, Japan). The pressure was maintained on the system for 1 h using constant pressure mode, followed by a slow pressure release through the column. The columns were then flushed with 95% acetonitrile for 1 h. After the washing, the columns were cut from the inlet side to desired lengths, 150 mm or 100 mm, and the new inlet of the columns was secured with one layer of frit.

The same packing procedure was applied for the column with 3 μm C_{18} particles (ODS AQ, YMC Europe, Scermbeck/Weselerwald, Germany), which was used for construction of the precolumn. The length of the precolumn was 1 cm and a frit was fitted at the inlet and the outlet ends as described above. The precolumn was secured between two stainless steel unions, 0.4 mm i.d. (SGE). Each end of the precolumn was inserted into the union and connected to a connection capillary (fused silica, 360 μm o.d. × 25 μm i.d.) with zero dead volume (Fig. 3). The inserted precolumn end and the connection capillary were secured by tightening a Vespel ferrule, 0.4 mm i.d. (SGE) around them. The connecting capillary was also secured by another Vespel ferrule at the other end of the union. The constructed precolumn was tested at high pressure (up to 320 atm; 1 atm = 101,325 Pa) before use.

2.4. Standards and sample preparation

A 10-peptide standard was prepared by dissolving the peptides in 2.1% formic acid to a concentration of 10 μg/ml for each peptide.

The BSA sample was tryptically digested according to the following scheme: approximately 250 μg of BSA was subjected to tryptic digestion. The protein was dissolved in 250 μl of 8 M urea, 0.4 M ammonium carbonate, followed by the addition of 10 μl of 45 mM dithiothreitol to reduce the disulfide bridges between cysteines. The mixture was incubated at 50 °C for 15 min and then cooled to ambient temperature. After the first incubation, 10 μl of 100 mM iodoacetamide was added and the sample was incubated for an additional 15 min at ambient temperature in darkness to irreversibly carbamidomethylate the cysteines. Finally, an amount of 10 μg (4%, w/w, protein) trypsin dissolved in 250 μl deionized water was added to the sample. The tryptic digestion was performed at 37 °C over night in darkness and the sample was then stored in at −80 °C. The digested BSA was diluted 20 times with 2.1% formic acid (mobile phase A) before the injection (7 μl).

2.5. Chromatography

Two LC systems were assembled for the experiments. These are denoted as LC systems I and II through the text. LC system I was used for all experiments with the peptide standards and LC system II was used for experiments with BSA (see Figs. 2 and 3). In both systems, a Varian HPLC system 9012 (Walnut Creek, CA, USA) was used for delivery of the mobile phases A (2.1% formic acid, pH 2) and B (2.1% formic acid, 90% acetonitrile). The LC systems delivered 600 nl/min after split of the mobile phases to a 150 mm length capillary column via a fused-silica transfer capillary (1 m × 19 μm i.d.). This capillary was used both as means for transporting the mobile phase and an on-line flow meter. The

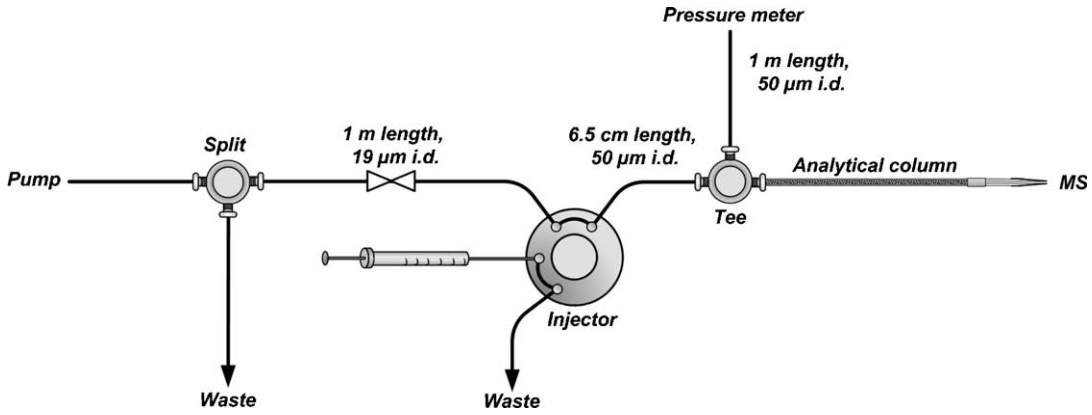

Fig. 2. Experimental set-up of the LC–MS system I. Column: 150 mm × 0.095 mm packed with 3 μm C_2/C_{18} particles, 120 Å pore size. For further details see Section 2.5.1.

pressure drop in the capillary was measured by connecting the outlet of the capillary to another Varian HPLC system. The pump's pressure meter was isolated and connected to the LC system via a fused-silica capillary (1 m × 50 μm i.d.). The measured pressure drop (ΔP) in the capillary is dependent on the flow rate (Q) through the system. The volumetric flow rate (Q) through the capillary can be expressed as:

$$Q = \frac{\pi \Delta P r_c^2}{8\eta L}$$

where r_c, L and η presenting the internal radius, the length of the capillary and the viscosity of the mobile phase, respectively [19]. This equation was used for calculation of the flow rate through the capillary. The effect of the surrounding temperature (measured with a thermometer) and composition of the mobile phase on viscosity were also considered in the calculation. The viscosity of the mobile phase was estimated by neglecting the presence of formic acid (2.1%) in the mobile phases and using the tabled reference values for acetonitrile–water mixtures [6]. The accuracy of the flow meter was tested by measurement of the flow rate in the system. The calculated flow rate was in good agreement with measured flow rate (<8% error).

2.5.1. LC system I

A schematic drawing of the set-up for LC system I is shown in Fig. 2. An electrically actuated four-port switching valve from Valco (Schenkon, Switzerland) with a 200 nl internal sample loop was used as the injector valve. The sample injection and collection of data from the mass spectrometer was started immediately after the start of the gradient program. The analytes in the peptide standards were concentrated on the front of the column, due to a delay time for the gradient to reach the column. A linear gradient

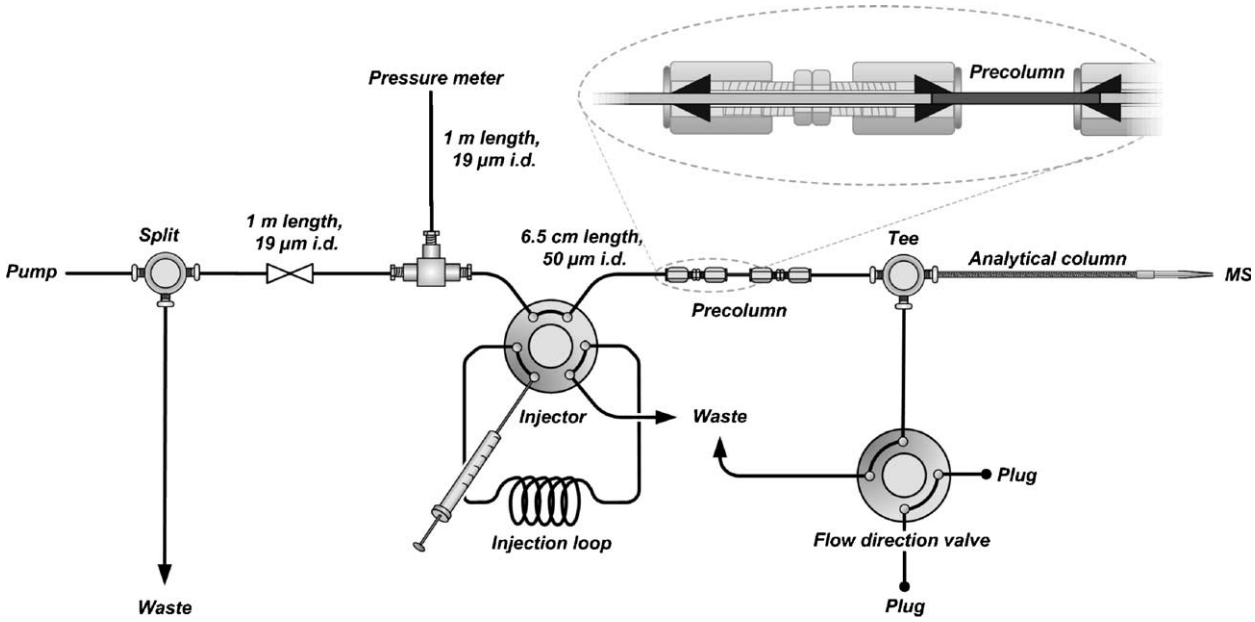

Fig. 3. Experimental set-up of the LC–MS system II. Precolumn: 10 mm × 0.095 mm packed with 10 μm C_{18} particles, 120 Å pore size. Analytical column: 100 mm × 0.095 mm packed with 3 μm C_2/C_{18} particles, 120 Å pore size. For further details see Section 2.5.2.

of 5% B to 60% B under 13 min was applied for the separation of the analytes. The program continued with 60% B for 5 min and finally 5% B for 12 min to reach equilibrium in the column before the next injection.

2.5.2. LC system II

A schematic drawing of the set-up for LC system II is shown in Fig. 3. An electrically actuated six-port switching valve from Valco with a 7 μl sample loop was used as the injector valve and a second electrically actuated four-port switching valve from Valco was used as the flow direction valve, which was connected via a tee between a 10 mm length precolumn and a 100 mm length capillary column. The flow direction valve was switched to its start position after equilibration of the column with 5% B (passing through the precolumn as well as column). The precolumn was equilibrated with 100% A for 3 min at a flow rate of 3.1 μl/min. The eluent from the precolumn was diverted from the column and directed into the waste by the flow direction valve during equilibration and the initial desalting step. The sample, diluted digested BSA, was injected immediately after start of the program. The analytes were concentrated and desalted on the precolumn. After 2.3 min, the injection loop was switched back to the start position. The desalting was continued for an additional 0.7 min, after which the flow direction valve blocked the flow path to the waste and the eluent was forced into the analytical column. The gradient program was also started at this time. A linear gradient of 0% B to 60% B under 60 min was applied to achieve separation of the analytes.

2.6. Mass spectrometry

All MS experiments were conducted with a Jaguar orthogonal time-of-flight (O-TOF-MS) instrument (Leco, St. Joseph, MI, USA). The instrument has a non-reflectron flight tube with a quadratic field profile, giving a resolution (FWHM) over 2000 for reserpine (609 *m*/*z*) and a mass range of 0–6000 *m*/*z*. The pulsing frequency was set to 5 kHz at a summing rate of 4800, resulting in a spectral acquisition of 1.04 spectra/s. The potential on the interface plate was set at 700 V and the flow of nitrogen curtain gas for the source region was set to 600 ml/min at a temperature of 100 °C. An *x*, *y*, *z*-micromanipulator (Protana, Odense, Denmark) in which a stainless steel tube, fitting 360 μm o.d. fused silica capillaries, provided the ESI potential for conductive coated tips. A positive ESI potential of 3.4–4.6 kV, depending on the LC configuration, was applied to the ESI emitter.

2.7. Study of flow rate effect on mass response

A Harvard Apparatus syringe pump, Model 11 (Harvard Apparatus, Holliston, MA, USA) was used for continuous infusion experiments. A 25 μl Hamilton gastight syringe (Hamilton, Reno, NV, USA) was coupled via a Peek union (Upchurch Scientific, Oak Harbor, WA, USA) to a 30 cm long fused silica electrospray emitter (25 μm i.d. × 360 μm o.d.) shaped and coated with "Black Dust" as described in Section 2.2.2. The position of the spray emitter and the ESI potential were carefully optimized for each flow rate. The experiments were performed from the lowest flow rate (150 nl/min) to the highest (2 μl/min). For each flow rate, the peptide concentration of the sample solution was increased from 0.1 to 100 μg/ml, followed by a thorough washing step. The ion current for the singly charged methionine–enkephalin at *m*/*z* 574.1–574.8 was monitored for 60 s for each experiment.

2.8. Safety considerations

All acids should be handled with great care. Acetonitrile is combustible, volatile and slightly toxic if exposed to lungs or skin. Trichloroethylene is toxic and potentially carcinogenic and protective gloves and glasses should be used. Polyimide sealing resin is a liquid irritant and should be handled using protective gloves and safety goggles. To avoid electrical chock, the high voltage power supplies should be handled with extreme care. The neuropeptides are biologically active and should be handled with care using protective gloves.

3. Result and discussion

One of the most important advantages of miniaturized LC is the low sample volume required when using a concentration sensitive detector. The required volume is inversely proportional to the square of the column internal diameter, thus reducing the i.d. results in a downscaling factor of $(d_1/d_2)^2$ for the injection volume [20]. However, this is only true if the ESI-MS acts as a concentration sensitive detector. Abian et al. [2] studied the influence of the flow rate on the response of the mass spectrometer for pure electrospray mass spectrometry. The behavior of the detector shifted from concentration sensitive to mass flow sensitive as the flow rate decreased. In this study of the band-broadening effects in nanoLC experiments, we wanted to establish the lowest flow rate were the MS still acts as a concentration sensitive detector. Therefore, continuous infusion experiments were performed, as described in the experimental section, where a peptide signal was monitored for different flow rates and concentrations. The median relative standard deviation for the different runs was 2.6% (ranging from 14.3–0.6%) with generally higher R.S.D. values for lower flow rates and concentrations. The flow rates 500 and 700 nl/min yielded the most stable signal.

The response for a certain concentration was taken as the peptide signal divided by the average value over all flow rates. Thereby the responses for the different concentrations were brought to the same level, and Fig. 4 shows the relation between response and flow rate for concentrations that span three orders of magnitude. For this particular combination of interface and mass spectrometer, the MS response decreased

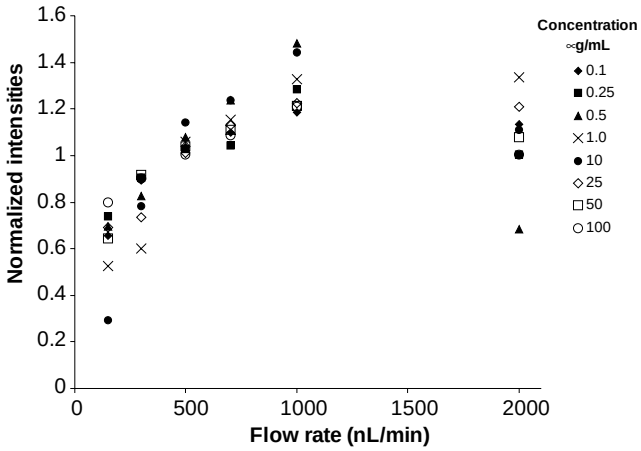

Fig. 4. Influence of the flow rate on the response of the mass spectrometer, using continuous infusion of methionine–enkephalin at different concentrations ranging from 0.1 to 100 μg/ml. The normalized intensity is calculated as the signal divided by the average signal over all flow rates. For each, the ESI potential and emitter position were optimized.

markedly at flow rates below 500 nl/min, which indicates mass sensitive behavior. This was valid for all concentrations and accordingly the subsequent nanoLC–MS experiments were performed at 600 nl/min.

3.1. Configuration studies

The performance of the configurations (A–D in Fig. 1) was investigated for LC system I (Fig. 2). Four different columns were used, denoted as columns 1–4 throughout the text. Columns 1 and 2 had integrated ESI emitter and were both used with configurations A and B, while columns 3 and 4 were regular columns with configurations C and D. Each set-up was a combination of a specific configuration and a specific column (A1, A2, B1, B2, C3, C4, D3, D4). Three replicated injections of 200 nl of a 10-peptide standard mixture were made for each set-up.

Fig. 5 shows typical chromatograms obtained for the different configurations. For each of the ten peptides the variables retention time (t_r), peak width at half-height (W), peak height (H) and peak area (A) were evaluated. These 40 variables were obtained from the three replicated injections on the various set-ups, in total $3 \times 8 = 24$ runs. Thus, the results comprised a data table with 40 columns (variables) and 24 rows (runs). Tables 1 and 2 show the contents of the first row and the last column, respectively. As a measure of the variations for each variable, the relative standard deviation was calculated. The R.S.D. values for the ten analytes were combined into a pooled R.S.D. value for each peak parameter, indicating the variation over all set-ups and replicates. In a similar way, the pooled R.S.D. values for pure replicates (within each set-up) were calculated as a measure of the random variations. The results were 3.4% (1.7%), 18.8% (9.7%), 51% (21%) and 50% (22%) for t_r, W, H and A, respectively (the values within parenthesis are for pure replicates, e.g. random variations).

3.2. Principal component analysis

In order to elucidate the data structure of the results, i.e. the systematic variation between the set-ups as monitored by

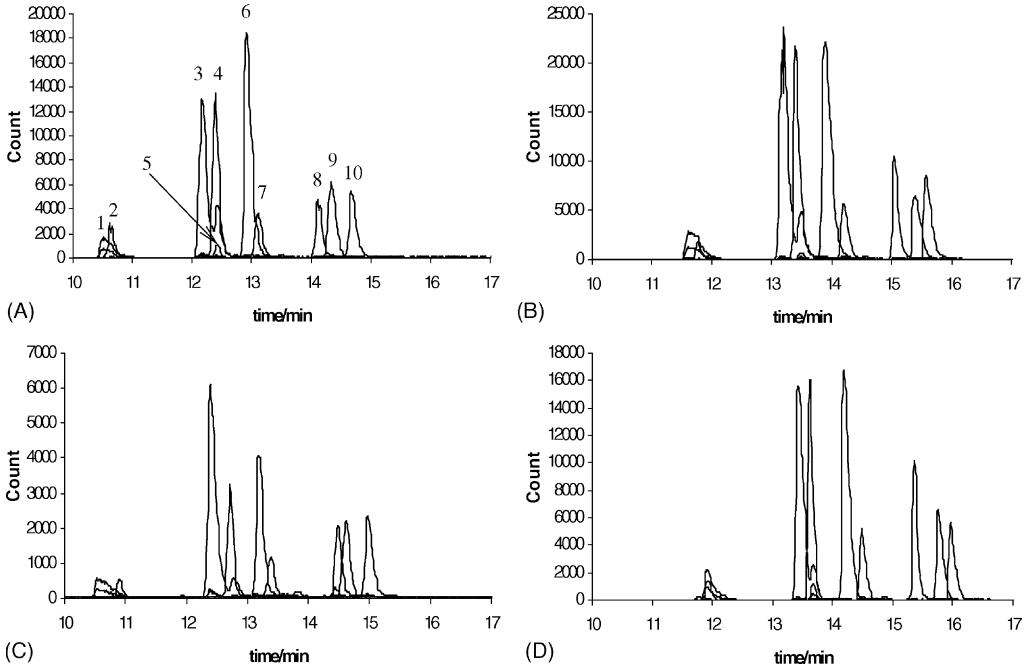

Fig. 5. Typical chromatograms obtained by injection of 10-peptide standard mixture using configurations A–D. (1) Bradykinin fragments 1–5, (2) Arg^8-vasopressin, (3) bradykinin, (4) LHRH, (5) oxytocin, (6) angiotensin II, (7) methionine–enkephalin, (8) bombesin, (9) leucine–enkephalin, and (10) substance P.

Table 1
Results from separation of 10-peptides using LC for set-up C3 (first replicate of three injections)

	Width at half-height (s)	Retention time (min)	Peak height	Peak area
Bradykinin fragment 1–5	13.5	11.95	2489.8	604.7
Arg^8-vasopressin	6.0	12.08	2077.9	229.2
Bradykinin	7.2	13.60	21089.5	3756.2
LHRH	5.9	13.81	18245.1	1968.6
Oxytocin	4.4	13.89	591.7	53.9
Angiotensin II	8.1	14.35	21992.1	3002.6
Methionine–enkephalin	8.7	14.66	3685.7	536.5
Bombesin	6.6	15.68	6769.7	863.2
Leucine–enkephalin	8.7	15.95	4932.1	749.7
Substance P	8.0	16.28	6948.6	1007.4

For details see Section 3.

Table 2
Peak width at half-height for substance P in the experiments (three replicates for each set-up)

Set-up	Width at half-height (s)	Set-up	Width at half-height (s)	Set-up	Width at half-height (s)	Set-up	Width at half-height (s)
A1	8.6	B1	7.9	C3	8.0	D3	6.6
A1	7.1	B1	8.1	C3	8.3	D3	6.8
A1	7.0	B1	8.2	C3	8.0	D3	7.2
A2	7.5	B2	8.5	C4	8.8	D4	12.1
A2	7.6	B2	8.5	C4	8.6	D4	12.4
A2	8.1	B2	7.6	C4	8.3	D4	9.3

the different peak parameters, a principal component analysis (PCA) was performed using the Unscrambler (CAMO A/S, Oslo, Norway). Prior to the analysis, all variables were centered and scaled to unit variance, thereby displaying uniform variations around zero regardless of the original range. This pre-processing of data (auto-scaling) resulted in the initial data table outlined in Fig. 6.

The principal components (PCs) are obtained as linear combinations of the scaled variables. Thus, a PC is given by a set of coefficients (*loadings*) that defines a weighted sum of the 40 variables (peak parameters). This sum is a single combined result (*score*) for each of the 24 rows (runs). The first PC is constructed so that the loadings (with unit square sum) result in maximum score variation between the runs. In that sense PC1 is the most informative linear combination of the peak parameters.

The first principal component can be associated with the dominating source of systematic variation between the different runs; due to different set-ups but also to possible changes in experimental conditions between replicates. The loadings reflect the variation pattern or 'profile', the manifestation in the peak parameters, while the scores describe how much of the 'profile' that is at hand for each run. Because of the centering of the original variables, the initial data refer to variations around the mean 'profile' of the original data and the scores will likewise assume positive and negative values with zero sum. Variables with high loadings are those most influenced by the cause of the PC1 pattern, either in the positive or negative direction (with positive or negative loading, respectively).

The PC1 *model* is simply the 'multiplication table' (or outer vector product) formed by the score column and the

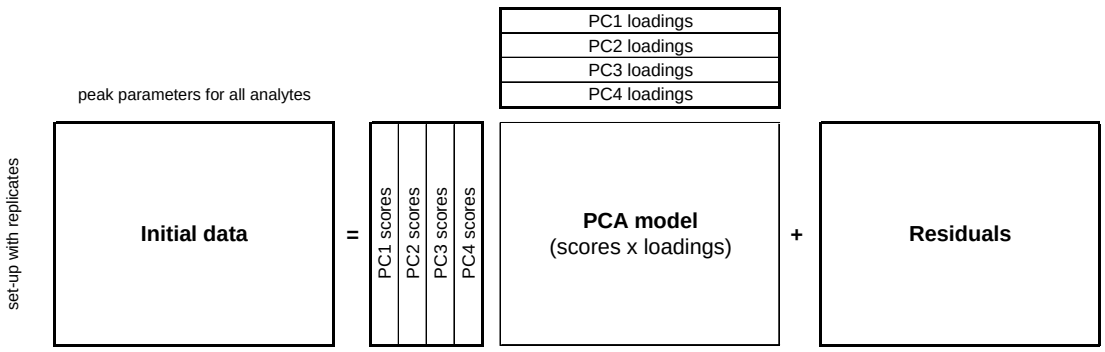

Fig. 6. Outline of PCA modeling. The initial data table is decomposed into a PCA model (scores × loadings) and a residual table, here with four principal components.

loading row. The differences between the initial data and the model constitute a residual table, which is minimized in the sense of least squares. This is a consequence of the inherent relation between the sums of squares (SS) for the three tables: SS (initial) = SS (PC1) + SS (residual). It can be shown that SS (PC1) equals the square sum of the score column, which was maximized by the PC procedure, and thereby SS (residual) is minimized. A certain amount of the initial variations is said to be explained by the PC1 model:

$$\frac{\text{SS (PC1)}}{\text{SS (initial)}} \times 100\%$$

The residual table can still contain structured data, i.e. reflect the influence of another source of systematic variations. Applying the same procedure as for the initial data on the residuals, results in the second principal component (PC2), with corresponding loadings and scores. By adding the two 'multiplication tables' a two-component PC model is obtained, with a higher amount of explained variance: SS (model) = SS (PC1) + SS (PC2), where SS (PC1) > SS (PC2). For each row (run) there are now two score values, and for each column (peak parameter) there are two loading values.

Still more PCs can be calculated and included in the model, thereby extracting more and more of the systematic variations in the data. The score columns and the loading rows are combined into the score and loading matrices, and the sum of 'multiplication tables' is obtained as the matrix product as outlined in Fig. 6. With four PCs, the model explained 89% of the total variation with the following contributions: PC1 = 45%, PC2 = 23%, PC3 = 17% and PC4 = 4%.

3.3. Interpretation of the PCA results and other findings

After PCA with four components, the runs as well as the peak parameters will each be characterized by four values: scores and loadings, respectively. A scatter plot of the PC1 and PC2 scores provides a highly informative visualization of the different runs, where the 40 peak parameters evaluated for each runs are reduced to (or projected onto) single points.

Fig. 7a shows the PC1/PC2 *score plot*, with the set-up designations as a marker for each run. Hence each set-up is represented by three points, corresponding to the three replicates. Now the distance between two runs in the two-dimensional map is a measure of the dissimilarity between the results (peak parameters), although different scales for the two axes must be considered. The systematic difference between the set-ups can be visually compared with

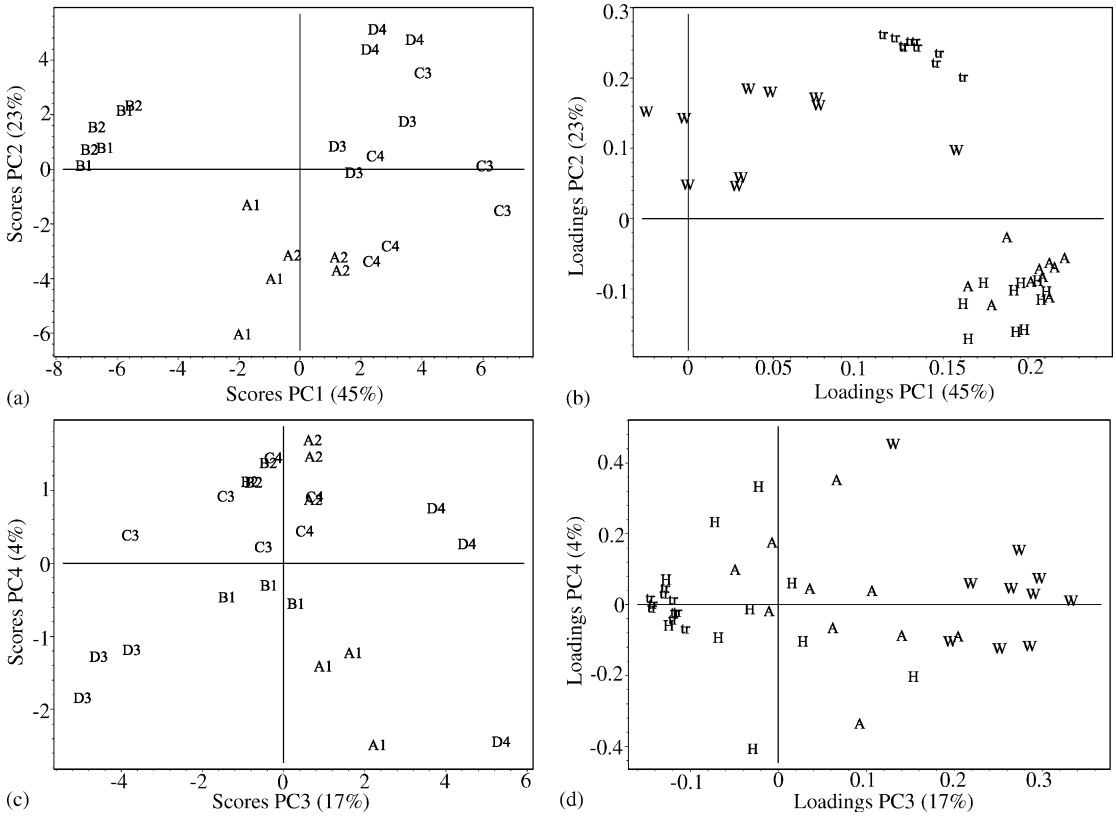

Fig. 7. Principal component analysis of auto-scaled data. Upper panel: (a) score plot and (b) loading plot for PC1 and PC2. Lower panel: (c) score plot and (d) loading plot for PC3 and PC4. Each experiment corresponds to a point in the score plots and each variable to a point in the loading plots. The markers used in the score plots are: A–D for the tip configuration and 1–4 for the column identity (with identical markers for the replicates). The markers used in the loading plots are: H, A, tr and w for of peak height, peak area, retention time and peak width at half-height of each peptide. For visual clarity, the identity of the individual peptides was not included in the designation.

the more random variations between the replicated runs. By the dual designation (configuration and column) it is also possible to judge separately the influence of both factors.

Fig. 7a shows that there is a clear clustering according to the configuration; especially the B configuration separates from the others with negative score values in the most prominent direction (PC1). In order to express this discrepancy in peak parameters rather than scores, the PC1/PC2 *loading plot* (Fig. 7b) must be considered. This plot shows that the more negative PC1 scores for configuration B corresponds to lower height (*H*) and area (*A*) for all peaks, as the these variables have high positive PC1 loadings. The clustering of the *H* and *A* parameters for all peaks implies that these quantities are closely correlated. Likewise, the retention times for all peaks are closely correlated, being shorter for the B configuration. Moreover, they have high positive loadings for PC2, hence associated with the spread of the scores in the PC2 direction. Here, it seems to be some systematic difference between configuration A (with shorter transition times) and the others. This pattern, however, is not as clear as that for configuration A versus the others in the PC1 direction.

The lower response (peak height and area) obtained with configuration B is probably due to the longer path between the spray tip and the electrical contact, resulting in a potential drop. This cannot be compensated for due to the limitations for the potential applied by the mass spectrometer (5 kV). There is also a correspondingly shorter path between the contact and ground (the injector), which leads to an increased current and possibly formation of bubbles at the contact by oxidation of water ($2H_2O \rightarrow 4H^+ + 4e^- + O_2$). Regardless of the cause, configuration B yielded an unstable spray, which was also observed by microscopic observation during the experiments.

The variations modeled by PC1 and PC2 are mainly associated with the configurations. The systematic column contributions (1–2 and 3–4, respectively) are less discernible; it is more like the individual set-ups are kept together with small variations between replicates. The PC1/PC2 variation is mainly monitored by the height, area and retention time, while the peak width is less influenced (except for that of the first peak, the right-most '*W*' in the loading plot). However, in the PC3/PC4 score plot (Fig. 7c) some clustering according to the column appears with column 1 to the left, column 3 downwards and column 4 upwards. For the individual set-ups the clusters are much tighter, hence the PC3/PC4 variations are mainly due to sources associated with the specific combination of configuration and source. Especially the large difference in PC3 scores for the D configuration with columns 3 and 4 could be noted. According to the PC3/PC4 loading plot, this difference is most clearly associated with the efficiency of the LC system as monitored by the peak widths (*W*). Actually, the same configuration (D) gave both the highest (small *W*) and the lowest (large *W*) efficiency dependent on the column (columns 3 and 4, respectively). On the other hand, with configuration C the column influence was hardly discernible.

The PCA results indicate that there is no decisive difference between the tested configurations regarding the efficiency of the LC system. Rather, each time an arbitrary configuration is assembled, the experimental skills of the operator determine the achieved efficiency. However, there is always a risk to introduce a post column dead volume with configurations C and D (separate emitter), and the risk is probably higher for configuration D because it is not possible to observe the connection between the column and the emitter. On the other hand, the observed difference between D3 and D4 in the PC3 direction (Fig. 7c) is associated with variations in retention time (t_r) as well as efficiency (*W*). According to the loading plot (Fig. 7d) these variations are negatively correlated (with different signs for the t_r loadings and *W* loadings, respectively). A difference in post column dead volume between D3 and D4 is not consistent with such a behavior; hence it is probably not the cause of the efficiency difference. In conclusion, introduction of post column dead volume at emitter mounting seems not to be a critical issue, at least not for the selected experimental conditions.

The configurations B and D are expected to be more sensitive to different mobile phases [16] and sample matrix. Davis et al. [21] reported formation of metal adduct ions with many peptides when using configuration D and making the electrical contact via metals such as stainless steel. They also observed, from time to time, formation of intense background while making the electrical contact via graphite ferrules. Finally, they eliminated these problems by making the electrical contact via a platinum sheath. However, we did not observe any metal adducts during our experiments using a stainless steel union, which might be due to poor sensitivities for such adducts, or be a result of passivation of the stainless steel surface [22].

Configuration A eliminates any risk for post column dead volume, which makes it more suitable for columns with even smaller internal diameter.

Configuration C has several advantages compare to the other configurations. This configuration is less sensitive to different mobile phases than configurations B and D. In addition, the emitter and the column can easily be replaced independently and connection point between the column and the emitter is visible through the transparent sleeve, which minimize the risk of any dead volume introduction in this point. Therefore, configuration C was chosen for the tryptic digest analysis.

3.4. Tryptic digest of BSA

A tryptic digest of BSA was chosen to represent a more complex sample. The digested BSA was first pre-concentrated and desalted on the precolumn and later separated on the analytical column with separate emitter (configuration C). The pre-concentration of the analytes on the precolumn were facilitated by omitting any organic solvent in the mobile phase A. The packing material, ODS-AQ, was chosen because it can be used with 100%

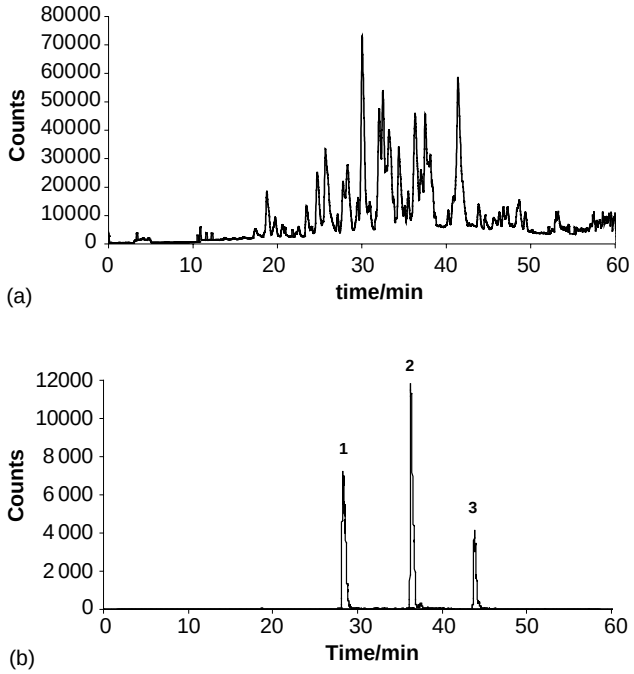

Fig. 8. Typical chromatogram obtained when analyzing 2.5 pmol injected BSA digest using configurations C. (a) Total ion chromatogram (50–1500 *m*/*z*). (b) Three arbitrary extracted ions showing *m*/*z*: (1) 417.2 (3 H^+), (2) 480.5 (3 H^+) and (3) 682.3 (3 H^+) corresponding to BSA fragments [35–44] (FKDLGEEHFK, M_r 1248.61), [360–371] (RHPEYAVSVLLR, M_r 1438.80) and [168–183] (RHPYFYAPELLYYANK, M_r 2044.02), respectively.

water as a mobile phase without experiencing stationary phase collapse [23].

The separation of the tryptic digest of BSA is shown in Fig. 8. A rapid identification of the digest was conducted by taking approximately 30 chromatographic peaks, evenly distributed throughout the chromatogram, and reduce their corresponding mass spectra to peptide masses. The peptide masses were submitted to Mascot using the peptide mass fingerprint search for matching possible tryptic fragments to the SwissProt database 42.4 (243,185 sequences, 137,300,669 residues). The search parameters were set to maximum two missed cleavage sites, carbamidomethylated cysteines and a peptide mass tolerance of ±0.5 u. The Mascot search rendered in only significant scores (above 65) for BSA precursors (P02769) with total scores ranging from 147 to 145 and 23 out of 33 masses could be assigned to BSA.

4. Conclusion

Four different approaches to perform nanoLC–MS have been evaluated in respect of obtained signal intensity, efficiency and stability. The principal component analysis clearly shows that the efficiency of a nanoLC system at a given flow rate is not influenced by the choice of configuration, i.e. if a minimal dead volume is assured. A configuration with a separate emitter and column is preferable, since independent replacement of either part can easily be made. Applying the ESI potential at the end of the emitter shows less dependency of mobile phase composition. In addition, this configuration can be coupled to the column with visually confirmed zero dead volumes. However, the integrated emitter column is preferable at lower flow rates, where the influences of post column dead volumes are pertinent.

Acknowledgements

The authors thank Andreas Pettersson for his help with graphics and Margareta Ramström for assistance with the tryptic digestion of BSA. The support of the Swedish Society for Medical Research, the Swedish Research Council Grant VR 629-2002-6821 and 621-2002-5261 (JB) is gratefully acknowledged. JB has a senior research position at the Swedish Research Council (VR).

References

[1] J.P.C. Vissers, J. Chromatogr. A 856 (1999) 117.
[2] J. Abian, A.J. Oosterkamp, E. Gelpí, J. Mass Spectrom. 34 (1999) 244.
[3] G. Hopfgartner, T. Wachs, K. Bean, J. Henion, Anal. Chem. 65 (1993) 439.
[4] A.J. Oosterkamp, E. Gelpí, J. Abian, J. Mass Spectrom. 33 (1998) 976.
[5] J.P.C. Vissers, H.A. Claessens, C.A. Cramers, J. Chromatogr. A 779 (1997) 1.
[6] L.R. Snyder, J.J. Kirkland, J.L. Glajch, Practical HPLC Method Development, Wiley, New York, 1997.
[7] K. Vanhoutte, W. Van Dongen, I. Hoes, F. Lemière, E.L. Esmans, H. Van Onckelen, E. Van den Eeckhout, R.E.J. van Soest, A.J. Hudson, Anal. Chem. 69 (1997) 3161.
[8] H.D. Meiring, E. Van der Heeft, G.J. ten Hove, A.P.J.M. de Jong, J. Sep. Sci. 25 (2002) 557.
[9] R. Swart, P. Koivisto, K.E. Markides, J. Chromatogr. A 828 (1998) 209.
[10] E. Gelpí, J. Mass Spectrom. 37 (2002) 241.
[11] L.J. Licklider, C.C. Thoreen, J. Peng, S.P. Gygi, Anal. Chem. 74 (2002) 3076.
[12] D.R. Barnidge, S. Nilsson, K.E. Markides, H. Rapp, K. Hjort, Rapid Commun. Mass Spectrom. 13 (1999) 994.
[13] M.R. Emmett, R.M. Caprioli, J. Am. Soc. Mass Spectrom. 5 (1994) 605.
[14] S. Nilsson, O. Klett, M. Svedberg, A. Amirkhani, L. Nyholm, Rapid Commun. Mass Spectrom. 17 (2003) 1535.
[15] S. Liu, W.J. Griffiths, J. Sjövall, Anal. Chem. 75 (2003) 1022.
[16] K. Vanhoutte, W. Van Dongen, E.L. Esmans, Rapid Commun. Mass Spectrom. 12 (1998) 15.
[17] S. Nilsson, M. Wetterhall, J. Bergquist, L. Nyholm, K.E. Markides, Rapid Commun. Mass Spectrom. 15 (2001) 1997.
[18] V.R. Meyer, Practical High Performance Liquid Chromatography, second ed., Wiley, New York, 1996.
[19] J.C. Giddings, Unified Separation Science, Wiley, New York, 1991.
[20] J.P. Chervet, M. Ursem, J.P. Salzmann, Anal. Chem. 68 (1996) 1507.
[21] M.T. Davis, D.C. Stahl, S.A. Hefta, T.D. Lee, Anal. Chem. 67 (1995) 4549.
[22] L. Konermann, E.A. Silva, O.F. Sogbein, Anal. Chem. 73 (2001) 4836.
[23] R. Wolcott, J.W. Dolan, LC–GC 17 (1999) 316.